Polarimetric Weather Radar: Overview of Principles and Applications

Branislav M. Notaroš, *Fellow, IEEE*

(Tutorial and Review)

***Abstract*—We introduce radar polarimetry, which generally is a less widely known concept of radar engineering, and explain the principles and applications of polarimetric Doppler weather radars. For example, a polarimetric radar can distinguish between precipitation particles of different shapes, compositions, and orientations. A relatively simple electromagnetic idea resulted in the 2012 upgrade of the National Weather Service network of 160 high-resolution Doppler weather radars in USA with dual-polarization technology. We describe the details of the Colorado State University CHILL research radar, featuring exceptional polarization purity and dual-frequency operation, and its setup and role in winter field experiments in Colorado, USA. We discuss several illustrative examples of polarimetric weather radar operations and observations and scattering calculations at different frequencies and in different climates. The radar signatures are discussed in relation to images and measurements by optical instrumentation on the ground. We present three distinct Colorado snowfall cases with fascinating polarimetric signatures at S-band and a rain event with C-band polarimetric scattering computations and measurements by the ARMOR research radar in Alabama, USA. Polarimetric weather-radar observations are crucial for understanding of microphysical properties of precipitation, and for development and use of numerical models for forecasting and climate projections.**

***Index Terms*—Electromagnetics; scattering; remote sensing; weather radar; radar meteorology; radar polarimetry; polarimetric Doppler radar; reflectivity; differential reflectivity; radar antennas; radar observations of snow and rain.**

I. Introduction

RADAR has been used for remote sensing of atmosphere, that is, for measurements of electromagnetic scattering from precipitation particles, practically since World War II [1]. Radar meteorology has since dramatically advanced based on multiple major scientific and engineering achievements and their synergies. A principal goal of weather radar observations is to relate the characteristics of measured scattered electromagnetic waves and fields to the microphysical properties of rain, snow or hail particles [2]. This is essential for numerical models for weather forecasting and regional climate modeling and simulations [3].

The principle of Doppler radar has found massive application in weather radar operations and observations since 1960s [4], [5]. This paper focuses on a less widely known concept, that of radar polarimetry, and more recent technology, that of dual-polarization or polarimetric weather radar [5]–[10]. Such a radar transmits well defined horizontally and vertically polarized electromagnetic waves or horizontal and vertical electric field components and measures the horizontal and vertical components of the scattered field. This thus produces the 2 × 2 scattering matrix, which relates the two orthogonal components of the scattered electric field to those of the incident field [11]. The polarimetric scattering properties of precipitation particles open a whole new level of analysis and information about the geometrical and microphysical properties of particles, as well as understanding of cloud processes and the resulting precipitation production and snow or water accumulation [6]–[34], For example, a polarimetric weather radar can distinguish between particles of different shapes, compositions, and orientations (e.g., rain vs. hail or rain vs. snow or snow aggregates vs. pristine crystal snowflakes) even in the Rayleigh regime, so even at the S-band (3 GHz), which is the frequency of operation of all National Weather Service (NWS) weather radars in USA. At S-band, precipitation particles are electrically small (much smaller in any linear dimension than the radar wavelength, which is 10 cm in free space), and electromagnetic scattering from such objects undergoes the Rayleigh regime. The "rule of thumb" criterion for Rayleigh precipitation scattering is: frequencies < 10 GHz, with a more precise judgment about the applicability of Rayleigh theory to the scattering from precipitation particles needing information on the size and composition of specific particles and precipitation [5], [35], [36]. Note that the dielectric constant is an important factor in determining whether this approximation is valid. Moreover, polarimetric weather radar is used for studying severe convective weather, such as tornadic supercells [37], [38].

Polarization diversity may include using any pair of "orthogonal" polarizations, including right- and left-hand circular polarizations [39]. Indeed, circularly polarized Doppler radars have been used in radar meteorology [40], especially in early stages of weather radar polarimetry [41], [9], as well as in non-meteorological applications [42]. Here, only radar measurements in the linear orthogonal polarization basis, based on horizontally and vertically polarized radiation, are considered, as a prevailing concept in radar meteorology [5]–[9]. This also includes polarimetry with transmitted or received elliptically polarized waves with known or measured horizontal and vertical components [9].

Manuscript received January 11, 2021; revised July 8, 2021, second revision October 6, 2021.

B. M. Notaroš, is with Colorado State University, Department of Electrical and Computer Engineering, Fort Collins, CO 80523-1373 USA (phone: 970-491-3537; e-mail: notaros@colostate.edu).

This paper introduces radar polarimetry, as a key component of radar meteorology, and explains the principles and applications of polarimetric Doppler weather radars, with some historical asides and a special attention to CHILL radar at Colorado State University (CSU), which features horizontal and vertical polarizations at two frequencies, in S- and X-bands. The paper discusses several examples of polarimetric weather radar operations and observations and scattering calculations, including three distinct cases during winter field experiments in Colorado, USA, with S-band measurements by CSU-CHILL radar as the principal research radar, as well as a rain event with C-band polarimetric scattering computations and measurements by the ARMOR radar in Alabama.

II. Radar Polarimetry: Need and Principles

Precipitation particles generally have non-spherical shapes; however, if a conventional (single-polarization) radar is used, radar measurements do not provide useful information about the shape and orientations of the particles; namely, that information is ambiguous. Indeed, based on the radar cross section and (single-polarization) reflectivity (Z) [6] (at horizontal or vertical polarization of the incident electric field), we cannot distinguish between the contributions to Z from the electrical size, shape, and orientation, respectively, of precipitation particles. Hence, a weather radar measuring Z is not able to distinguish between scattering from, for example, hailstones and raindrops, as illustrated in Fig. 1, assuming the same electrical size [43].

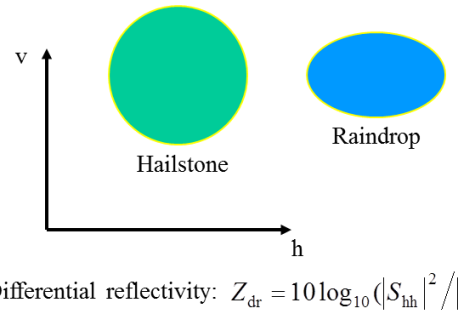

Fig. 1. A sketch illustrating, more conceptually than quantitatively, a rationale for using polarimetric weather radar: two precipitation particles of different shapes and orientations have noticeably different differential reflectivities (Z_{dr}), observed by a polarimetric or dual-polarization (h and v) radar, whereas reflectivities (Z), measured by a standard (e.g., horizontally polarized) Doppler weather radar, do not provide enough information for distinguishing between the two shapes/orientations (hailstone and raindrop) [43].

However, in dual-polarization (h and v) radar operation, a polarimetric radar is used to measure differential reflectivity, Z_{dr}, of precipitation, expressing how the reflectivity at horizontal polarization differ from that at vertical polarization [44]. Specifically, Z_{dr} is obtained as $Z_{dr} = 10\log_{10}(|S_{hh}|^2 / |S_{vv}|^2)$, with 'h' and 'v' referring to a horizontally and vertically polarized electromagnetic wave (its electric field vector), respectively, and S_{hh}, S_{hv}, S_{vh}, and S_{vv} being the elements of the 2 × 2 scattering matrix, relating E_h and E_v components of the scattered electric field to those of the incident field [6]. The two indices on the matrix elements refer to the polarization states of the transmitted and received radiation. A polarimetric weather radar thus provides additional information about shape and orientation of particles. Namely, Z_{dr} of the hailstone and that of the raindrop in Fig. 1 are different, and so are Z_{dr} values of snowflakes of different shapes. Another important polarimetric radar measurable is linear depolarization ratio, $\mathrm{LDR} = 10\log_{10}(|S_{vh}|^2 / |S_{hh}|^2)$, and the full set of most frequently used polarimetric radar variables are Z_h (horizontal reflectivity), Z_{dr}, LDR, K_{dp} (specific differential phase), and ρ_{hv} (co-polar correlation coefficient) [6], [53]. Many other polarimetric variables have also been measured or calculated, for example, the specific differential attenuation, A_{dp}, relating the forward scattering amplitude at horizontal and vertical polarizations, used, for instance, to distinguish between large rain drops and melting hail as observed by a C-band radar in intense storms [14]. Note that for a sphere, or a spherical approximation (equivalent sphere with the same volume) of a precipitation particle, $Z_{dr} = 0$ dB and LDR → −∞ (dB).

III. Striking Historical Example: Fort Collins Flood

As a striking "historical" example of the importance of polarimetric weather radar operation, Figure 2 shows the radar-based estimation of rain rate (accumulation) and the precipitation gauge survey of rainfall for the city of Fort Collins, Colorado, on 28 July 1997, during the infamous Fort Collins Flood. This was a flash flood, where a heavy rain turned the ankle-deep Spring Creek flowing through central Fort Collins into a deadly river, "the water reached over heads, its strong current carried cars from roads and pulled people from their doorsteps or out of the grasp of loved ones" [45], causing five fatalities and huge material damage in the city and CSU campus, including the newly-constructed university library.

This event produced heavy cumulative rainfall from lots of small raindrops, an atypical situation for Colorado, where fewer, larger drops is a more common situation, namely, where drops form by the melting of hail and graupel particles [43]. This could not be observed by a standard (single-polarization) weather radar (NWS WSR-88D radars at the time) but only with a polarimetric radar (CSU-CHILL research radar), as can be seen in Fig. 2, where a polarimetrically tuned reflectivity–rain rate (Z–R) power law compared well with the gauge measured rainfall across the city, while a WSR-88D standard Z–R grossly underestimated the rain accumulation. Namely, small raindrops are spherical, whereas larger ones become oblate as in Fig. 1 (actually, rather flattened on the bottom), and such non-spherical shapes, in turn, are distinguishable by a polarimetric radar. One can speculate that if the NWS had dual-polarization radar capability in its radar network in 1997, more accurate radar-based precipitation estimation could have provided a flash flood warning that could, in turn, have saved the lost lives and prevented some of the property damage in the Fort Collins Flood.

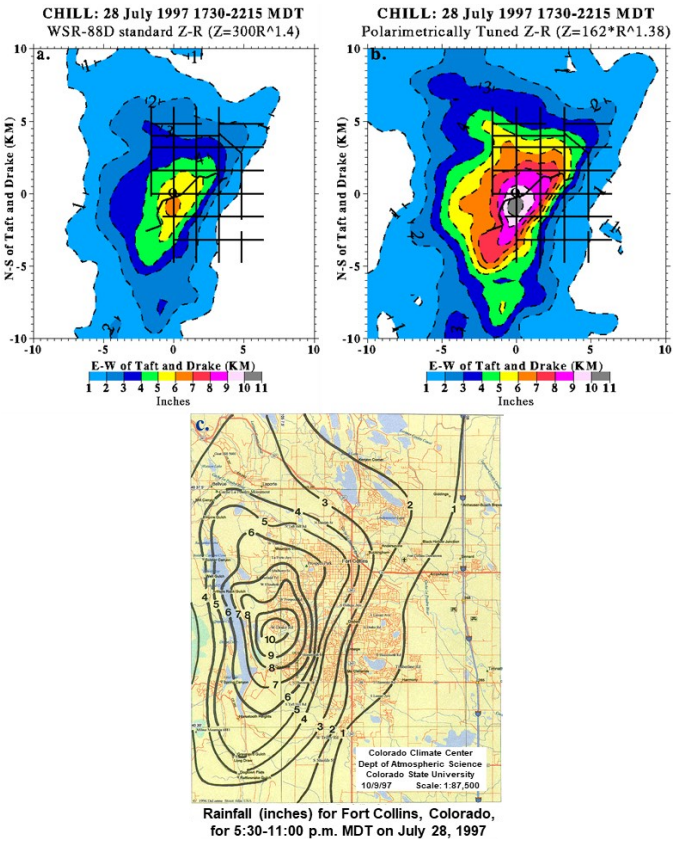

Fig. 2. A "historical" example of the importance of polarimetric (Fig. 1) weather radar operation: radar-based estimation of rain rate (accumulation) observed by CSU-CHILL radar operating in (a) standard (single-polarization) radar regime (National Weather Service WSR-88D radars at the time) and (b) dual-polarization regime (unique CSU-CHILL research radar capability at the time), and (c) precipitation gauge survey of rainfall – across the city of Fort Collins, Colorado, on 28 July 1997, during the infamous Fort Collins Flood, a devastating flash flood causing five fatalities and large material damage [45], [43].

IV. NEXRAD Network of 160 Polarimetric Doppler Weather Radars

Prof. V.N. Bringi, co-Principal Investigator of the MASCRAD project (see Fig. 6) and a pioneer of polarimetric radar meteorology [44], [6] "spent decades working with what he describes as a relatively simple idea to perfect the complex technology and to convince experimental radar meteorologists that it could be used in operational forecasting. His efforts paid off and his legacy was written when the NWS announced in 2011 that it would be upgrading its nationwide network of 159 Doppler weather radars with dual-polarization technology. The National Severe Storms Laboratory states that the potential benefits with dual polarization will be as significant as the nationwide upgrade to Doppler radar in the 1980s" [46]. Figure 3 shows the upgraded NWS network of currently 160 high-resolution S-band polarimetric Doppler weather radars.

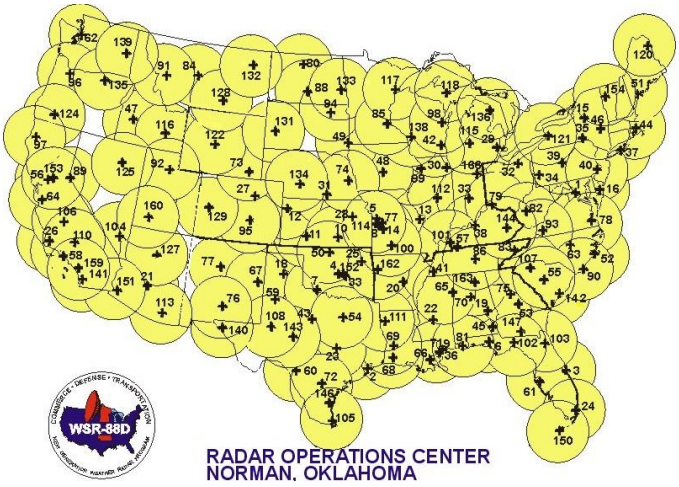

Fig. 3. Next-Generation Radar (NEXRAD) network of 160 high-resolution S-band Doppler weather radars operated by the US National Weather Service (NWS) and National Oceanic and Atmospheric Administration (NOAA) Radar Operations Center, in Norman, Oklahoma. In 2012, the NWS upgraded all of the WSR-88D (Weather Surveillance Radars–1988 Doppler) radars of the NEXRAD system with dual-polarization technology (see Figs. 1 and 2). (Source: US National Weather Service, Public domain)

Overall, radar polarimetry nowadays plays an absolutely essential role in weather research and meteorology. Indeed, polarimetric radar signatures in rain, snow, and hail storms with widely-differing precipitation particle classes, shapes, sizes, and compositions are distinct and fascinating, as well as extremely useful [12]–[34].

V. Dual-Frequency, Dual-Polarization CSU-CHILL Research Radar

The Colorado State University CHILL radar, Fig. 4, is a two-transmitter, two-receiver S-band dual-polarization system. Interestingly, the name of the radar (CHILL) was derived from "CHicago ILLinois radar" in 1970 when the radar was first assembled, and it was kept the same after the facility was moved from Illinois to Colorado in 1990. The current radar antenna is an 8.5-m dual-offset Gregorian reflector system, Fig. 4(a), with exceptional polarization purity and very low side lobes (< −35 dB) in any direction. The radar can measure LDR levels as low as −40 to −43 dB [47]. The antenna is housed inside an inflatable radome, shown in Fig. 4(b).

Another unique feature of the CSU-CHILL radar is its capability to collect dual-polarization data while operating in dual-frequency mode, with the same antenna reflector system [48]. This is enabled by a two-frequency, two-polarization antenna feed, shown in Fig. 4(c), which allows radar operation at both S-band (3 GHz) and X-band (9 GHz), either at one frequency at the time or simultaneously at both frequencies. With the same reflector system at both frequencies, the main (3-dB) beam-width of the antenna comes out to be 1.0° at 3 GHz and 0.33° at 9 GHz, as depicted in Fig. 5.

With this, for example, larger precipitation particles can, at the same time and within the same observation, appear to the radar as electrically small, i.e., in the Rayleigh regime (at 3 GHz), and as of a size comparable to the wavelength (at 9 GHz), where the elements of larger particles (relative to the

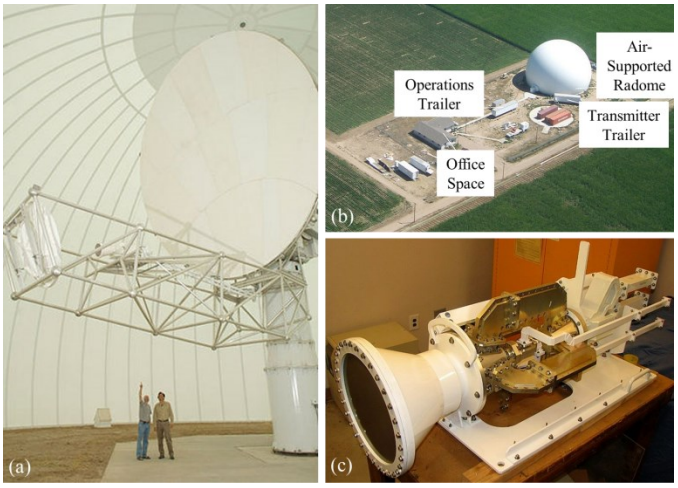

Fig. 4. CSU-CHILL radar, Colorado: (a) CHILL's dual-offset Gregorian parabolic reflector antenna and positioner system, (b) CHILL's antenna inflatable radome and transmitter and operations trailers, and (c) dual-polarization (h and v), dual-frequency (S- and X-bands) horn antenna feed for the reflector antenna system in (a), with the output of a magnetron transmitter being split to enable simultaneous radiation of both h and v polarized electromagnetic waves [47], [48], [43].

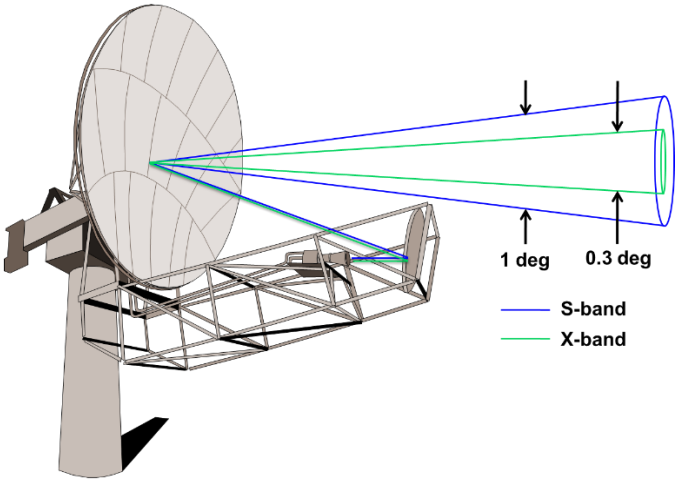

Fig. 5. Sketch illustrating radiation patterns at S- and X-bands of the CSU-CHILL radar antenna in Fig. 4(a) [48], [43].

wavelength) scatter with different phases, potentially producing large variances in the backscatter at each polarization. The Rayleigh and non-Rayleigh scattering behaviors, respectively, at the two frequencies, can be compared together providing additional information about the precipitation. In addition, propagation through rain, snow or hail at different frequencies undergoes different attenuations, which can also be used for observation and analysis. Note that differential attenuation at each polarization, as well as differential phase shifts during propagation, also provide information on the particle shapes, sizes, and number distributions [14]. Overall, dual-wavelength scattering and propagation information, provided by dual-wavelength radars, has many uses in atmospheric science research and meteorological practice [48], [49].

VI. Application of Polarimetric Radars in MASCRAD Snow Field Campaign 2014–2017

MASCRAD (MASC + Radar) winter field experiments were conducted in Colorado, USA, from 2014–2017. The campaign featured combined radar and in-situ observations and analyses of geometrical, microphysical, and scattering properties of snowfall [50]–[56], as depicted in Fig. 6. The primary radar for the campaign was the CSU-CHILL radar (Fig. 4), with added observations from National Center for Atmospheric Research (NCAR) SPOL radar, which is a state-of-the-art dual-polarization S-band weather research radar [57]. In-situ surface instruments were placed within a wind shield, at a field site at Easton Airport, near Greeley, Colorado (Fig. 6) [50]. The instrumentation included multi-angle snowflake camera (MASC) [51], [52] two-dimensional video disdrometer (2DVD) [50], [55], and mobile sounding equipment for launching radiosondes into atmosphere [50].

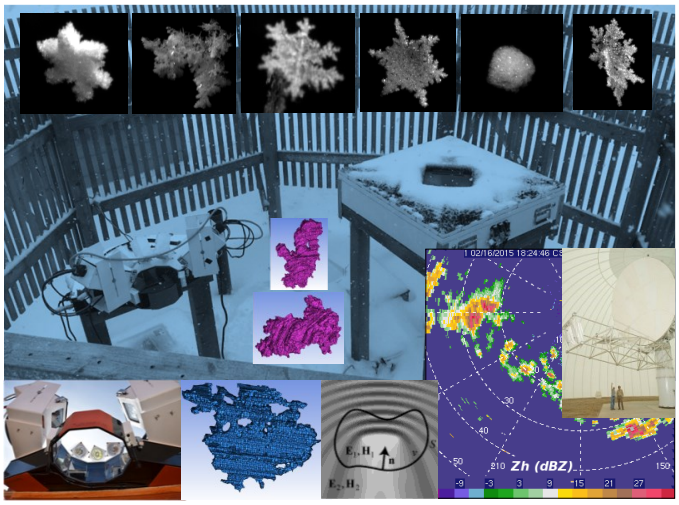

Fig. 6. MASCRAD snow field campaign 2014–2017, Colorado, USA [50]. The CSU-improved multi-angle snowflake camera (MASC) (photos on the left) is used to capture high-resolution images of snowflakes in free-fall (images at the top), along with their fall speeds [51], [52]. A visual hull method is used for 3D shape reconstruction of precipitation particles by processing the images captured by the MASC (meshes at the center and bottom) [51]. Polarimetric scattering (Fig. 1) analysis based on the method of moments (MoM) in conjunction with the surface integral equation (SIE) formulation (sketch at the bottom) is carried out on the reconstructed meshes [53]. A two-dimensional video disdrometer (2DVD) (photo on the right), collocated with the MASC, provides 2D contours of a particle, along with the fall speed and other important parameters [50], [55]. We use the fall speed, along with environmental conditions measured at the instrumentation site, to estimate the particle mass (Böhm's method), and then the effective dielectric constant of particles, based on a Maxwell-Garnet formula [51]. We develop geometrical, microphysical, and scattering models of natural snowflakes using the MASC, 2DVD, visual hull, and MoM-SIE, and tie them with CSU-CHILL radar (Fig. 4) observations (bottom-right) [50], [55], [56].

The location of the MASCRAD site relative to the CSU-CHILL and NCAR-SPOL radars is shown in Fig. 7; it is at 171.3° azimuth and 12.92 km range from CHILL. When selecting the surface instrumentation site, our principal goal was to minimize the influence of the ground clutter for the operation of CSU-CHILL, as our primary radar [50]. The goal

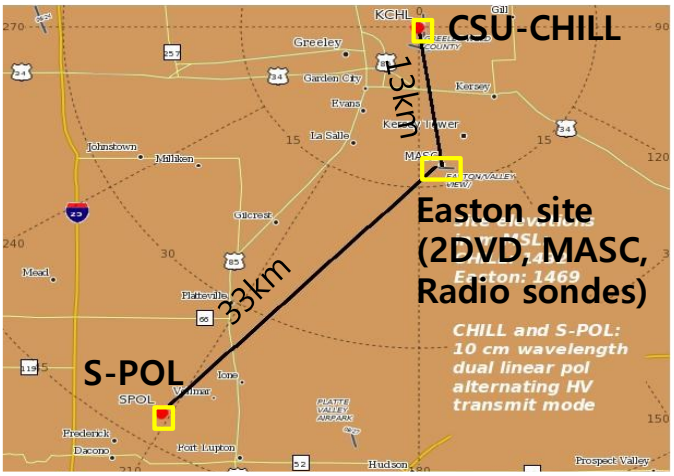

Fig. 7. MASCRAD radar observations were made by two ~10-cm wavelength, dual-polarization systems: CSU-CHILL and NCAR-SPOL, located, respectively, ~13 km and ~33 km away from the surface instrumentation site (in Fig 6). CSU-CHILL radar includes an X-band system as well, and can operate in dual-frequency mode (Fig. 4) [50].

was to enable as low elevation angles of the radar as possible, allowing for the antenna beam (in Fig. 5) to be as close as possible to the measurement volumes of the surface-based optical instruments at the site. This maximally reduces the vertical separation between the radar pulse sample volume and the MASC and 2DVD and thus makes the measurements of the snow by the optical instruments maximally relevant with respect to the observations of the snow in the radar volume aloft. On the other hand, when the elevation angle is too low, meteorological data collected by the radar becomes contaminated due to ground clutter. The MASCRAD site being on a ridge is ~32 m higher than the CSU-CHILL base, and the South Platte River valley with reduced terrain heights is located in between (Fig. 8). This allows clutter-free data collection by the radar at antenna beam elevations down to only 0.9° over the instrumentation site. At the ~13 km range (Fig. 7) and 0.9° elevation, the main beam of the CSU-CHILL antenna at X-band, being 0.33° wide (Fig. 5), illuminates a radar volume between 150 m and 224 m above ground level at the site.

For MASCRAD operations, prescribed sequences of high spatial and temporal resolution CHILL radar scans focusing on the MASCRAD Field Site (Fig. 6) were run, with a typical sequence including a 50° plan position indicator (PPI) volume sweep with the lowest clutter-free elevation angle of 0.9°. Two range height indicator (RHI) scans on azimuths that bordered the Easton site, at 171° and 172°, were also done [50], [56]. This combination of PPI and RHI scans was repeated at 3 minute intervals, and a cycle was usually augmented by three fixed pointing beam measurements with dwell of 20 seconds each.

Additionally, the KFTG WSR-88D radar located near Denver (Colorado) and the KCYS WSR-88D radar in Cheyenne (Wyoming) of the NWS NEXRAD dual-polarization S-band Doppler weather radar network (Fig. 3) were used as valuable secondary resources for validating or complementing CHILL and SPOL data.

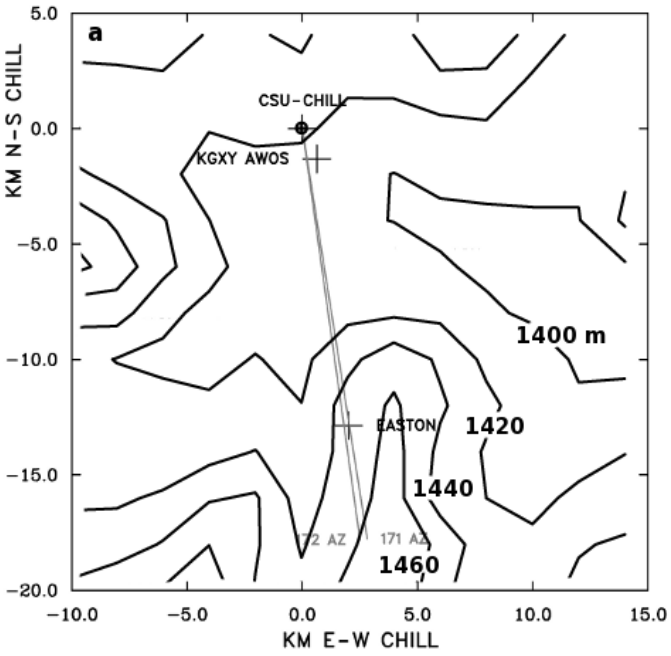

Fig. 8. Terrain height contours (m MSL) around the CSU-CHILL radar and the MASCRAD Field Site at Easton, used for evaluation of ground clutter between the radar and the instrumentation site. The radar azimuths bordering the Easton site (in Fig. 6) are shown in grey [56].

VII. Illustrative Examples of Polarimetric Radar Observations from Colorado and Alabama

As the first example of polarimetric weather radar observations, shown in Fig. 9 is the vertical profile of CSU-CHILL radar (Fig. 4) S-band data at 19:32 UTC on 16 February 2015 over the MASCRAD Field Site (Figs. 6–8) during a snow event with a documented graupel shower [55]. Details on obtaining the radar height profile data are given in [55]. We observe from the figure that the measured horizontal reflectivity and differential reflectivity near the surface and below 2 km to surface were about $Z_h \approx 25$ dBZ (rather high) and $Z_{dr} \approx -0.2$ dB (slightly negative), respectively, and then Z_h decreased and Z_{dr} increased rapidly with height from 2 km upward to, for instance, $Z_{dr} \approx 0.8$ dB (positive) and very low Z_h levels around 3.5 km height. Such a vertical profile with negative Z_{dr} values in the high Z_h areas along a vertical column is indicative of graupel particles of lump type below 2 km. On the other hand, the positive Z_{dr} and low Z_h at higher altitudes signify the likely predominance of pristine crystals as particle type. The conversion of pristine crystals to graupel particles between the two regions occurred via riming, an ice crystal growth process characterized by supercooled water droplets being collected at the surface of ice crystals. Particle riming represents an important microphysical process that affects the particle fall speed and microwave backscattering properties, measured by a radar [54], [56]. This conclusion about transformation of pristine crystals into graupel by riming is supported by meteorological analysis of sounding data. Moreover, images of particles collected by the MASC and 2DVD at the surface (Fig. 6) showed graupel particles, as in Fig. 10, where the measured fall speeds and densities of particles were typical for graupel as well. Finally, microwave

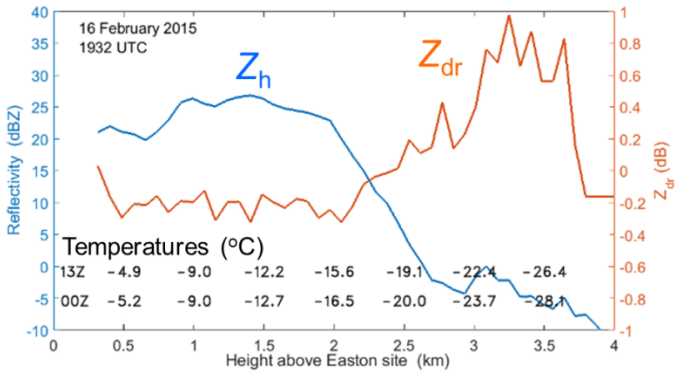

Fig. 9. Height profiles of horizontal reflectivity (Z_h) and differential reflectivity (Z_{dr}) (Fig. 1) using the CSU-CHILL radar (Fig. 4) S-band channel averaged across ± 0.25 km range interval of the MASCRAD Field Site (Figs. 6–8) during a graupel shower event on 16 February 2015. Temperatures from MASCRAD sounding (upper row) and NWS Denver sounding (lower row) are given at 0.5 km height intervals along the abscissa [55].

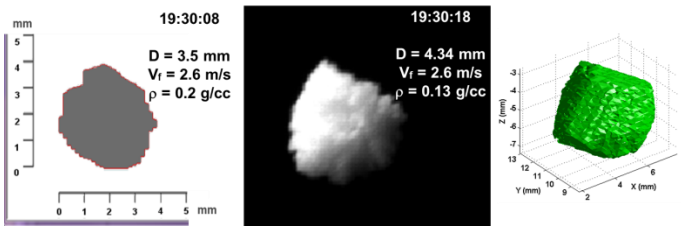

(a) (b) (c)

Fig. 10. Sample graupel images from (a) the 2DVD (Fig. 6) and (b) the MASC (Fig. 6) collected at the MASCRAD Field Site (Figs. 6–8) at ~19:30 UTC on 16 February 2015. The equi-volume spherical diameter (D), fall speed, and density of the particles measured by the instruments are also shown. (c) Visual hull 3D shape reconstruction (Fig. 6) based on the five MASC images of the particle in (b).

backscatter calculations confirmed slightly negative Z_{dr} values, as those measured by the radar, resulting from the shapes and orientations of graupel particles observed by the MASC and 2DVD [55].

The second example is a major snow band passage across the MASCRAD Field Site on 21 February 2015, with very high reflectivity (Z_h) values in excess of 30 dBZ [50]. In the lowest ~1 km from the surface, differential reflectivity (Z_{dr}) was consistently near 0 dB. Characteristic MASC images are shown in the inset of Fig. 11. These were typically relatively large-diameter rimed aggregates, and the concentrations of images (and particles) were high, which is consistent with the observed high Z_h values. However, these aggregates exhibited irregular shapes and orientations, which explains measured Z_{dr} values near 0 dB. Figure 11 shows a comparison of radar Z_{dr} and linear depolarization ratio (LDR) values observed in the graupel shower and snow band, on 16 and 21 February 2015, respectively. Both events exhibit Z_{dr} encompassing small positive and negative values (around 0 dB), with the histogram of the 16 February case, with graupel particles per MASC data, being distinctly skewed to the negative Z_{dr} range. On the other hand, the 21 February case shows slightly higher LDR levels, which can be attributed to the large aggregates having more irregular shapes that are further away from the sphere, as recorded by the MASC in the snow band [50].

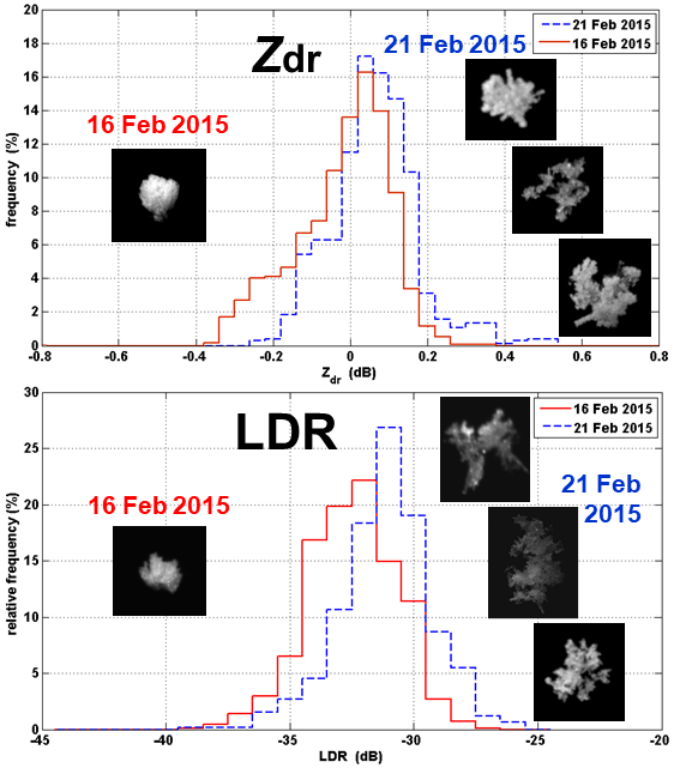

Fig. 11. CHILL radar (Fig. 4) measured S-band Z_{dr} and LDR (linear depolarization ratio) (see Section II) histograms for the 16 February 2015 graupel (Figs. 9 and 10) and 21 February 2015 snow band cases at the MASCRAD Field Site (Figs. 6–8) (data from [50]). Sample MASC (Fig. 6) images captured during each of the events are also shown.

The third example is a dissipating light snow area event of 3 March 2015 at and around the MASCRAD site, with low reflectivity (single digit positive Z_h values) and markedly positive Z_{dr} (exceeding +5 dB at times), as shown in Fig. 12 [50]. A low Z_h is indication of low concentrations of particles (provided that the particles are not very small), and when the particles are in small numbers, they collide and aggregate less

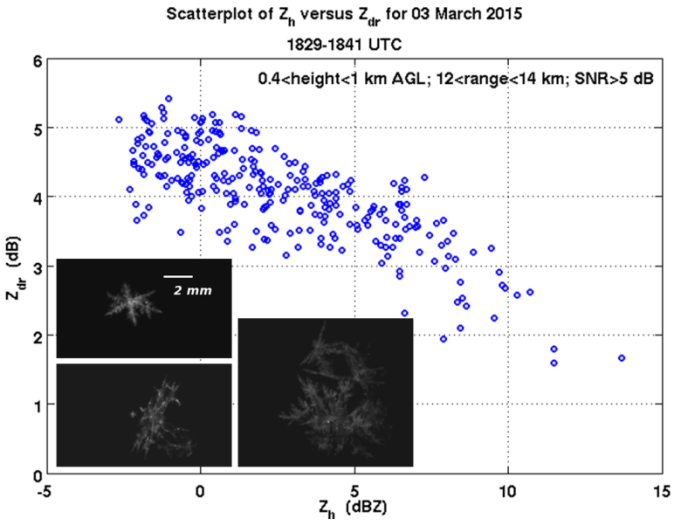

Fig. 12. Z_h vs. Z_{dr} (Fig. 1) scatterplot measured by the CHILL radar (Fig. 4) at S-band during a positive Z_{dr} in dissipating light snow area event on 3 March 2015 at the MASCRAD Field Site (Fig. 6). Selected MASC images are shown as well [50].

frequently. With minimal "aggregational" collisions occurring, the Z_{dr} near the ground is evidently positive as is intrinsic for individual crystals. In other words, the pristine, single crystals growing at higher altitudes with cooler temperatures maintain their flat aspect ratios and positive Z_{dr} as they descend, with infrequent collisions, to the ground. Indeed, individual crystal components are more readily apparent in the selected MASC images shown in the inset of Fig. 12 when compared, for example, to the heavily rimed aggregates of the 21 February 2015 snow band case in Fig. 11, indicating that there may be at least a mixture of pristine particles and aggregates that can produce the observed radar values [50].

The fourth example is a rain event that occurred on 25 December 2009 in Huntsville, Alabama, USA, with C-band polarimetric observations by ARMOR radar, shown in Fig. 13(a) [58], and ground measurements by a two-dimensional video disdrometer (Fig. 6) [59]. 2DVD measurements showed that a significant fraction of the raindrops were undergoing asymmetric mode oscillations, depicted in Fig. 13(b), which were attributed to frequent, and sustained, drop collisions [60]. Scattering calculations for 10,233 larger asymmetric drops over a 100-minute period were performed using the method of moments (MoM) for solving surface integral equations (SIEs) [59], [53] based on drop 3D shapes reconstructed from the collected 2DVD images, as illustrated in Fig. 13(c) [61]. Figure 14 shows an excellent agreement between polarimetric scattering calculations on a drop-by-drop basis at C-band [59] and the radar measurements, which is a remarkable result given a large volume at a considerable height of radar observed raindrops compared to ground observations within a disproportionately smaller measurement volume by the 2DVD [62].

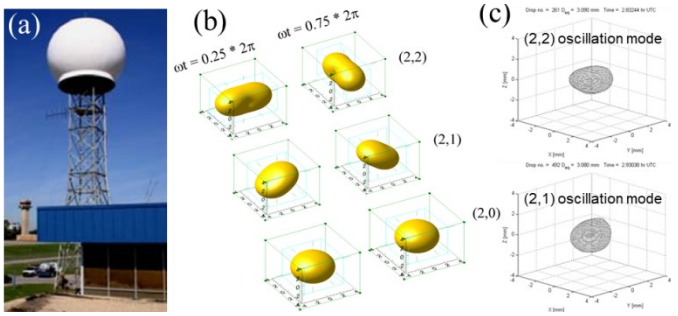

Fig. 13. (a) ARMOR (Advanced Radar for Meteorological and Operational Research) C-band (5.625 GHz) polarimetric Doppler weather radar, operated by the University of Alabama-Huntsville (UAH) and National Space Science and Technology Center (NSSTC) in Hunstfille, Alabama, USA [58]. (b) 3D views of the three fundamental oscillation modes, for two phases of the oscillation cycle, of asymmetric raindrops resulting from collision-induced drop oscillations (all units are mm) [60]. (c) 3D shapes of two raindrops, in different oscillation modes, reconstructed using two perpendicular drop contours from 2DVD (Fig. 6) measurements [61] during a rain event on 25 December 2009 in Huntsville, Alabama. The 2DVD site is at ~15 km range from the radar, the lowest elevation angle of the radar antenna is 1.3°, and the radar resolution volume is at ~340 m from the surface at this elevation [62].

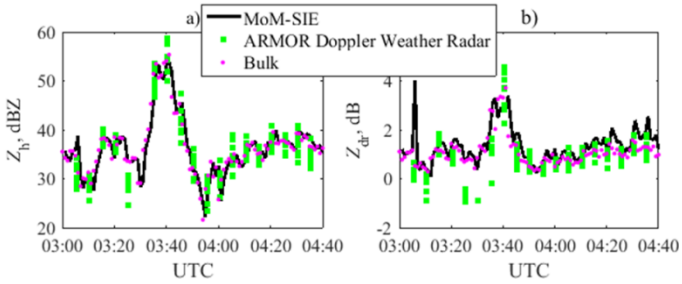

Fig. 14. Scattering computations and radar measurements at 5.625 GHz of (a) reflectivity (Z_h) and (b) differential reflectivity (Z_{dr}) (Fig. 1) over a period of 100 minutes during the 25 December 2009 rain event in Huntsville, Alabama [59]. Measurements are by the dual-polarization C-band ARMOR radar [Fig. 13(a)]. Scattering calculations are by the MoM-SIE technique (Fig. 6) based on integration over each 1-minute period using MoM-SIE drop-by-drop (for scattering amplitudes of individual drops), with MoM-SIE models reconstructed from 2DVD images [Fig. 13(c)], as well as by the T-matrix scattering code referred to as the bulk method [59].

VIII. Conclusion

This paper has explained the principles and applications of polarimetric Doppler weather radars, including some historical asides, with a special attention to CSU-CHILL radar, its components and capabilities, and its setup and role in MASCRAD winter field experiments in Colorado, USA, from 2014–2017. Radar polarimetry is a key enabling methodology and technology of radar meteorology, which, in turn, is absolutely essential for accurate and reliable weather forecasts.

The paper has discussed several illustrative examples of polarimetric weather radar operations and observations and scattering calculations at different frequencies and in different climates. The dual-polarization radar signatures have been discussed in relation to images and measurements by optical instrumentation, namely, the multi-angle snowflake camera and two-dimensional video disdrometer, on the ground. We have presented three MASCRAD snowfall cases featuring widely-differing meteorological settings that involved contrasting snowflake forms and compositions, such as graupel, heavily rimed aggregates, and pristine crystals. These contrasting snowflake classes strongly influenced S-band polarimetric radar observables, measured by the CSU-CHILL radar, which were hence used to characterize precipitation and its impacts in various cases. This included correlation of radar measurements with MASC and 2DVD images and comparison of the results from different cases. We have presented a comparative study of dual-polarization radar measurements at C-band of rainfall, by the ARMOR radar, in Alabama, USA, and the associated polarimetric scattering calculations, by the MoM-SIE method, of 2DVD shape reconstructed asymmetric raindrops resulting from collision-induced mixed-mode drop oscillations.

As an additional example, which is a part of current and future analysis work of the international community, Fig. 15 provides an illustration of the use of polarimetric radars within international winter field experiments conducted in conjunction with the Winter Olympics 2018, in South Korea, namely, International Collaborative Experiments for Pyeongchang 2018 Olympic and Paralympic Winter Games

(ICE-POP 2018). Shown in Fig. 15 are the list and locations of ICE-POP2018 radars, where the radar sites were selected to minimize beam blockage due to the mountainous terrain over the supersites with ground instrumentation allowing for radar measurements within 200-400 m above the surface. The analyses of radar and surface data collected during the ICE-POP 2018 are ongoing.

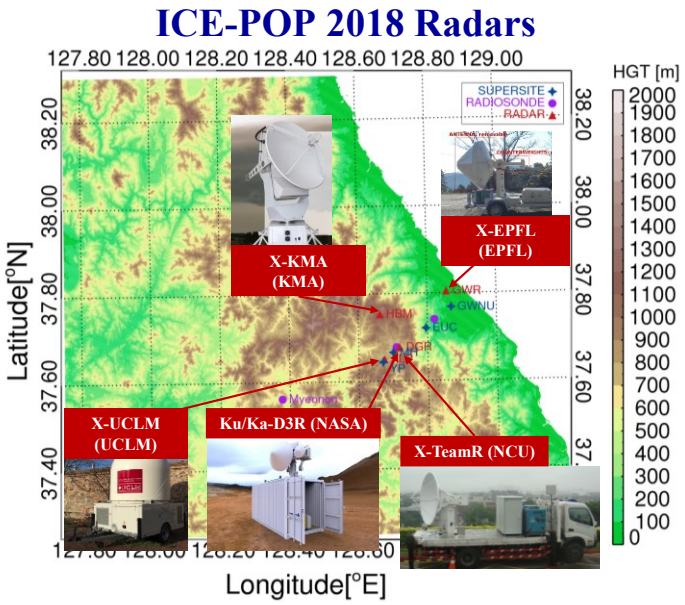

Fig. 15. Unique composition of radars for the International Collaborative Experiments for Pyeongchang 2018 Olympic and Paralympic Winter Games (ICE-POP 2018), South Korea: location of four X-band dual-polarization Doppler radars (from four institutions/agencies in Asia and Europe) and NASA's dual-polarization, dual-wavelength (K_u,K_a)-band radar (D3R) [63], [49] across Winter Olympics 2018 venues, in Pyeongchang region on Korean peninsula.

Polarimetric scattering observables (e.g., Z_{dr} and LDR) and dual-polarization radar measurements and calculations of scattering from precipitation are a vital prerequisite for detailed understanding of microphysical properties of snow, rain or hail particles and for radar-based quantitative precipitation estimation. They are crucial for enhancing our understanding of cloud processes and the resulting precipitation production and snow/water accumulation, and feed directly into development, validation, improvement, and use of numerical models for cloud and precipitation simulations, forecasting, and regional climate projections.

Overall, the goals of the paper are to introduce radar polarimetry, which generally is a less widely known concept of radar technologies and applications, to describe the electromagnetic and engineering background of dual-polarization radar, to show how invaluable its use and impact are in meteorology and atmospheric science, and to discuss some fascinating polarimetric radar signatures in snow and rain storms. However, polarimetric Doppler radar can be used for dual-polarization measurements of scattering from non-precipitation particles and objects as well, with multitude of potential applications in detection, evaluation, and analysis of various targets [64], [65], which, of course, do not need to be small at all. Examples include the use of polarimetric radar for healthcare sensing [42], as well as dual-polarization radar observations of biological targets (e.g., insects, birds, and bats) [66]–[68], smoke and ash from fires or volcanoes [69]–[71], tornadic debris [72], ground and sea clutter [73], [74], and military chaff [75]. Finally, there are significant improvements in radar polarimetry coming from advances in signal processing techniques and architectures – for example, a multiple-input multiple-output (MIMO) radar with instantaneous radar polarimetry [76].

Acknowledgements

This work was supported by the US National Science Foundation under grants AGS-1344862, AGS-1431127, and AGS-2029806 and by NASA PMM Science grant NNX16AE43G. The author would like to thank his collaborators and students: Prof. V. N. Bringi, Patrick Kennedy, Dr. Merhala Thurai, Dr. Gwo-Jong Huang, Dr. Andrew J. Newman, Prof. GyuWon Lee, Dr. John Hubbert, Cameron Kleinkort, Dr. Sanja B. Manić, Dr. Elene Chobanyan, and Adam Hicks. The author is also grateful to Prof. Steven A. Rutledge, Scientific Director of CSU-CHILL National Radar Facility, for providing the presentation of [43] from which Figs. 1, 2, 4, and 5 were adapted, and to Prof. GyuWon Lee, Principal Investigator of ICE-POP 2018, for providing Fig. 15.

References

[1] D. Atlas, Ed., "Radar in Meteorology," *American Meteorological Society*: Boston, USA, 1990.

[2] J. Leinonen, D. Moisseev, and T. Nousiainen, "Linking snowflake microstructure to multi-frequency radar observations," *Journal of Geophysical Research*, Vol. 118, 2013, pp. 3259–3270.

[3] A. J. Heymsfield, S. Y. Matrosov, and N. B. Wood, "Toward Improving Ice Water Content and Snow-Rate Retrievals from Radars. Part I: X and W Bands, Emphasizing CloudSat," *J. Appl. Meteor. Climatol*., Vol. 55, 2016, pp. 2063–2090.

[4] R. Lhermitte, "Application of pulse Doppler radar technique to meteorology.," *Bull Amer. Meteor. Soc*., Vol. 47, 1966, pp. 703-711.

[5] R. J. Doviak and D. S. Zrnic, "Doppler Radar and Weather Observations," 2nd edition, *Academic Press*: San Diego, USA, 1993.

[6] V. N. Bringi and V. Chandrasekar, "Polarimetric Doppler Weather Radar: Principles and Applications," *Cambridge University Press*, 2001.

[7] A. Ryzhkov and D. S. Zrnic, "Radar Polarimetry for Weather Observations," *Springer*: Chaim, Switzerland, 2019.

[8] G. Zhang, "Weather Radar Polarimetry," *CRC Press*: Boca Raton, Florida, USA, 2017.

[9] V. Bringi and D. Zrnic, "Polarization Weather Radar Development from 1970–1995: Personal Reflections," *Atmosphere*, Vol. 10, No. 11, 2019, p. 714.

[10] R. M. Rauber and S. W. Nesbitt, "Radar Meteorology: A First Course," *John Wiley and Sons*: Hoboken, New Jersey, USA, 2018.

[11] A. Kostinski and W. Boerner, "On foundations of radar polarimetry," *IEEE Trans. Antennas Propag*., Vol. 34, no. 12, 1986, pp. 1395–1404.

[12] E. M. Griffin, T. J. Schuur, A. V. Ryzhkov, H. D. Reeves, and J. C. Picca, "A Polarimetric and Microphysical Investigation of the Northeast Blizzard of 8–9 February 2013," *Wea. Forecasting*, Vol. 29, 2014, pp. 1271–1294.

[13] A. V. Ryzhkov and D. S. Zrnic, "Discrimination between Rain and Snow with a Polarimetric Radar," *J. Appl. Meteor*., Vol. 37, 1998, pp. 1228–1240.

[14] M. Thurai, E. Chobanyan, V. N. Bringi and B. M. Notaros, "Large Raindrops Against Melting Hail: Calculation of Specific Differential Attenuation, Phase and Reflectivity," *Electronics Letters*, Vol. 51, No. 15, 2015, pp. 1140–1142.

[15] A. V. Ryzhkov, S. E. Giangrande, and T. J. Schuur, "Rainfall estimation with a polarimetric prototype of WSR-88D," *J. Appl. Meteor*., Vol. 44, 2005, pp. 502−515.

[16] M. Thurai, V. N. Bringi, and W. A. Petersen, "Rain microstructure retrievals using 2-D video disdrometer and C-band polarimetric radar," *Adv. Geosci*., Vol. 20, 2009, pp. 13−18.

[17] V. N. Bringi, C. R. Williams, M. Thurai, and P. T. May, "Using dual-polarized radar and dual-frequency profiler for DSD characterization: A case study from Darwin, Australia," *J. Atmos. Ocean. Tech.*, Vol. 26, 2009, pp. 2107−2122.

[18] P. Tabary, G. Vulpiani, J. J. Gourley, A. J. Illingworth, R. J. Thompson, and O. Bousquet, "Unusually High Differential Attenuation at C Band: Results from a Two-Year Analysis of the French Trappes Polarimetric Radar Data," *J. Appl. Meteor. Climatol.*, Vol. 48, 2009, pp. 2037–2053.

[19] C. C. Crowe, C. J. Schultz, M. R. Kumjian, L. D. Carey, and W. A. Petersen, "Use of dual-polarization signatures in diagnosing tornadic potential," *Electron. J. Oper. Meteor.*, Vol. 13, 2012, pp. 57-78.

[20] M. Thurai, V. N. Bringi, L. D. Carey, P. Gatlin, E. Schultz and W. A. Petersen, "Estimating the accuracy of polarimetric radar-based retrievals of drop size distribution parameters and rain rate: An application of error variance separation using radar-derived spatial correlations," *J. Hydrometeor.*, Vol. 13, 2012, pp. 1066−1079.

[21] L. D. Carey and W. A. Petersen, "Sensitivity of C-band polarimetric radar–based drop size estimates to maximum diameter," *J. Appl. Meteor. Climatol*., Vol. 54, 2015, pp. 1352–1371.

[22] C. Sandford, A. Illingworth, and R. Thompson, "The Potential Use of the Linear Depolarization Ratio to Distinguish between Convective and Stratiform Rainfall to Improve Radar Rain-Rate Estimates. *J. Appl. Meteor. Climatol.,* Vol. 56, 2017, pp. 2927–2940.

[23] J. Straka, D. S. Zrnić, and A. V. Ryzhkov, "Bulk hydrometeor classification and quantification using polarimetric radar data: Synthesis of Relations," *J. Appl. Meteor*. Vol. 39, 2000, pp. 1341–1372.

[24] D. S. Zrnić, A. Ryzhkov, J. Straka, Y. Liu, and J. Vivekanandan, Testing a procedure for automatic classification of hydrometeor types. *J. Atmos. Oceanic Technol*., Vol. 18, 2001, pp. 892–913.

[25] P. C. Kennedy and S. A. Rutledge, "S-Band Dual-Polarization Radar Observations of Winter Storms," *J. Appl. Meteor. Climatol.*, Vol. 50, 2011, pp. 844–858.

[26] G. Zhang, S. Luchs, A. Ryzhkov, M. Xue, L. Ryzhkova, and Q. Cao, "Winter Precipitation Microphysics Characterized by Polarimetric Radar and Video Disdrometer Observations in Central Oklahoma," *J. Appl. Meteor. Climatol*., Vol. 50, 2011, pp. 1558–1570.

[27] J. Andrić, M. R. Kumjian, D. S. Zrnić, J. M. Straka and V. M. Melnikov, "Polarimetric Signatures above the Melting Layer in Winter Storms: An Observational and Modeling Study," *J. Appl. Meteor. Climatol*., Vol. 52, 2013, pp. 682–700.

[28] R. Bechini, L. Baldini, and V. Chandrasekar, "Polarimetric Radar Observations in the Ice Region of Precipitating Clouds at C-Band and X-Band Radar Frequencies," *J. Appl. Meteor. Climatol*., Vol. 52, 2013, pp. 1147–1169.

[29] M. R. Kumjian, A. V. Ryzhkov, H. D. Reeves, and T. J. Schuur, "A Dual-Polarization Radar Signature of Hydrometeor Refreezing in Winter Storms," *J. Appl. Meteor. Climatol*., Vol. 52, 2013, pp. 2549–2566.

[30] M. Schneebeli, N. Dawes, M. Lehning, and A. Berne, "High-resolution vertical profiles of X-band polarimetric radar observables during snowfall in the Swiss Alps," *J. Appl. Meteor. Climatol*., Vol. 52, 2013, pp. 378–394.

[31] R. S. Schrom, M. R. Kumjian, and Y. Lu, "Polarimetric Radar Signatures of Dendritic Growth Zones within Colorado Winter Storms," *J. Appl. Meteor. Climatol*., Vol. 54, 2015, pp. 2365–2388.

[32] G. Skofronick-Jackson, D. Hudak, W. Petersen, S. W. Nesbitt, V. Chandrasekar, S. Durden, K. J. Gleicher, G. Huang, P. Joe, P. Kollias, K. A. Reed, M. R. Schwaller, R. Stewart, S. Tanelli, A. Tokay, J. R. Wang, and M. Wolde, "Global Precipitation Measurement Cold Season Precipitation Experiment (GCPEX): For Measurement's Sake, Let It Snow," *Bull. Amer. Meteor. Soc*., Vol. 96, 2015, pp. 1719–1741.

[33] A. Ryzhkov, P. Zhang, H. Reeves, M. Kumjian, T. Tschallener, S. Trömel, and C. Simmer, "Quasi-Vertical Profiles—A New Way to Look at Polarimetric Radar Data," *J. Atmos. Oceanic Technol*., Vol. 33, 2016, pp. 551–562.

[34] G. Zhang, V. N. Mahale, B. J. Putnam, Y. Qi, Q. Cao, A. D. Byrd, P. Bukovcic, D. S. Zrnic, J. Gao, M. Xue, Y. Jung, H. D. Reeves, P. L. Heinselman, A. Ryzhkov, R. D. Palmer, P. Zhang, M. Weber, G. M. Mcfarquhar, B. Moore III, Y. Zhang, J. Zhang, J. Vivekanandan, Y. Al-Rashid, R. L. Ice, D. S. Berkowitz, C. Tong, C. Fulton, and R. J. Doviak, "Current Status and Future Challenges of Weather Radar Polarimetry: Bridging the Gap between Radar Meteorology/Hydrology/Engineering and Numerical Weather Prediction," *Adv. Atmos. Sci.*, Vol. 36, 2019, pp. 571–588.

[35] R. J. Hogan, L. Tian, P. R. A. Brown, C. D. Westbrook, A. J. Heymsfield, and J. D. Eastment, "Radar Scattering from Ice Aggregates Using the Horizontally Aligned Oblate Spheroid Approximation," *Journal of Applied Meteorology and Climatology*, Vol. 51, No. 3, 2012, pp. 655-671.

[36] J. Tyynelä, J. Leinonen, C. D. Westbrook, D. Moisseev, D., and T. Nousiainen, "Applicability of the Rayleigh-Gans approximation for scattering by snowflakes at microwave frequencies in vertical incidence," *J. Geophys. Res. Atmos.*, Vol. 118, 2013, pp. 1826–1839.

[37] R. M. Wakimoto and V. N. Bringi, "Dual-polarization observations of microbursts associated with intense convection: The 20 July storm during the MIST project," *Mon. Wea. Rev*., Vol. 116, 1988, pp. 1521–1539.

[38] R. J. Hogan, P. R. Field, A. J. Illingworth, R. J. Cotton, and T. W. Choularton, "Properties of embedded convection in warm-frontal mixed-phase cloud from aircraft and polarimetric radar," *Quart. J. Roy. Meteor. Soc*., Vol. 128, 2002, pp. 451–476.

[39] E. Torlaschi and A. R. Holt, "A comparison of different polarization schemes for the radar sensing of precipitation," *Radio Science*, Vol. 33, No. 5, 1998, pp. 1335-1352.

[40] M. Galletti, D. Huang and P. Kollias, "Zenith/Nadir Pointing mm-Wave Radars: Linear or Circular Polarization?," *IEEE Transactions on Geoscience and Remote Sensing*, Vol. 52, No. 1, 2014, pp. 628-639.

[41] B. L. Barge and G. A. Isaac, "The Shape of Alberta Hailstones," *J. Rech. Atmos.,* Vol. 7, 1973, pp. 11–20.

[42] Y. He, C. Gu, H. Ma, J. Zhu and G. V. Eleftheriades, "Miniaturized Circularly Polarized Doppler Radar for Human Vital Sign Detection," *IEEE Transactions on Antennas and Propagation*, Vol. 67, No. 11, 2019, pp. 7022-7030.

[43] S. A. Rutledge, "Innovative Radar Research at CSU," College of Engineering Innovation Series, March 25, 2015, *Colorado State University*, CSU Denver Center, Denver, CO.

[44] T. A. Seliga and V. N. Bringi, "Potential Use of Radar Differential Reflectivity Measurements at Orthogonal Polarizations for Measuring Precipitation," *J. Appl. Meteor*., Vol. 15, 1976, pp. 69–76.

[45] E. Udell, "Spring Creek Flood anniversary: Revisit the deadly night," *The Coloradoan*, Fort Collins, Colorado, July 20, 2017.

[46] The American Meteorological Society, "2012 Remote Sensing Prize Winner Sees Polarimetric Radar Research Go Nationwide," *The Front Page*, Boston, MA, January 26, 2012.

[47] V. N. Bringi, R. Hoferer, D. A. Brunkow, R. Schwerdtfeger, V. Chandrasekar, S. A. Rutledge, J. George, and P. C. Kennedy, "Design and Performance Characteristics of the New 8.5-m Dual-Offset Gregorian Antenna for the CSU–CHILL Radar," *J. Atmos. Oceanic Technol*. Vol. 28, 2011, pp. 907–920.

[48] F. Junyent, V. Chandrasekar, V. N. Bringi, S. A. Rutledge, P. C. Kennedy, D. Brunkow, J. George, and R. Bowie, "Transformation of the CSU-CHILL Radar Facility to a Dual-Frequency, Dual-Polarization Doppler System," *Bull. Amer. Meteor. Soc*., Vol. 96, 2015, pp. 975–996.

[49] G.-J. Huang, V. N. Bringi, A. J. Newman, G. Lee, D. Moisseev, and B. M. Notaros, "Dual-Wavelength Radar Technique Development for Snow Rate Estimation: A Case Study from GCPEx," *Atmospheric Measurement Techniques*, Vol. 12, 2019, pp. 1409–1427.

[50] B. M. Notaros, V. N. Bringi, C. Kleinkort, P. Kennedy, G.-J. Huang, M. Thurai, A. J. Newman, W. Bang, and G. Lee, "Accurate Characterization of Winter Precipitation Using Multi-Angle Snowflake Camera, Visual Hull, Advanced Scattering Methods and Polarimetric Radar," *Invited Paper*, Special Issue "Advances in Clouds and Precipitation," *Atmosphere*, Vol. 7, No. 6, June 2016, pp. 81–111.

[51] C. Kleinkort, G.-J. Huang, V. N. Bringi, and B. M. Notaros, "Visual Hull Method for Realistic 3D Particle Shape Reconstruction Based on High-Resolution Photographs of Snowflakes in Free Fall from Multiple Views," *J. Atmos. Oceanic Technol*., Vol. 34, March 2017, pp. 679–702.

[52] G.-J. Huang, C. Kleinkort, V. N. Bringi, and B. M. Notaros, "Winter precipitation particle size distribution measurement by Multi-Angle Snowflake Camera," *Atmospheric Research*, Vol. 198, 2017, pp. 81–96.

[53] E. Chobanyan, N. J. Sekeljic, A. B. Manic, M. M. Ilic, V. N. Bringi, and B. M. Notaros, "Efficient and Accurate Computational Electromagnetics Approach to Precipitation Particle Scattering Analysis Based on Higher-Order Method of Moments Integral Equation Modeling," *J. Atmos. Oceanic Technol*., Vol. 32, October 2015, pp. 1745–1758.

[54] A. Hicks and B. M. Notaros, "Method for Classification of Snowflakes Based on Images by a Multi-Angle Snowflake Camera Using Convolutional Neural Networks," *J. Atmos. Oceanic Technol*., Vol. 36, December 2019, pp. 2267– 2282.

[55] V. N. Bringi, P. C. Kennedy, G.-J. Huang, C. Kleinkort, M. Thurai, and B. M. Notaros, "Dual-polarized radar and surface observations of a winter graupel shower with negative Z_{dr} column," *J. Appl. Meteor. Climatol*., Vol. 56, February 2017, pp. 455–470.

[56] P. Kennedy, M. Thurai, C. Praz, V. N. Bringi, A. Berne, and B. M. Notaros, "Variations in Snow Crystal Riming and Z_{DR}: A Case Analysis," *J. Appl. Meteor. Climatol*., Vol. 57, 2018, pp. 695–707.

[57] J. C. Hubbert, P. Kennedy, V. Chandrasekar, S. Rutledge, W.C. Lee, V. N. Bringi, J. Wilson, D. Brunkow, M. Dixon, T. Weckwerth, J. George, E. Loew, J. Van Andel, A. Phinney, B. Bowie, B. Rilling, and S. Ellis, "FRONT: The Front Range Observational Network Testbed," Presented at *92nd AMS Annual Meeting*, January 22-26, 2012, New Orleans, LA.

[58] W. A. Petersen, K. Knupp, J. Walters, R. Blakeslee, W. Deierling, M. Gauthier, M. Newchurch, and R. McNider, "The NSSTC ARMOR C-Band Dual-Polarimetric Doppler Radar: A Tool for Integrated Remote Sensing," *Huntsville Simulation Conference*, International Society for Modeling and Simulation, 26-27 October 2005, Huntsville, Alabama.

[59] S. B. Manic, M. Thurai, V. N. Bringi, and B. M. Notaros, "Scattering Calculations for Asymmetric Raindrops during a Line Convection Event: Comparison with Radar Measurements," *J. Atmos. Oceanic Technol*., Vol. 35, June 2018, pp. 1169–1180.

[60] M. Thurai, V. N. Bringi, A. B. Manic, N. J. Sekeljic, and B. M. Notaros, "Investigating rain drop shapes, oscillation modes, and implications for radiowave propagation," *Radio Sci.*, Vol. 49, 2014, pp. 921-932.

[61] M. Thurai, S. Manic, M. Schönhuber, V. N. Bringi, and B. M. Notaros, "Scattering Calculations at C-band for Asymmetric Raindrops Reconstructed from 2D Video Disdrometer Measurements," *J. Atmos. Oceanic Technol*., Vol. 34, April 2017, pp. 765–776.

[62] M. Thurai, P. Gatlin, V. N. Bringi, W. Petersen, P. Kennedy, B. Notaros, and L. Carey, "Toward Completing the Raindrop Size Spectrum: Case Studies Involving 2D-Video Disdrometer, Droplet Spectrometer, and Polarimetric Radar Measurements," *J. Appl. Meteor. Climatol*., Vol. 56, April 2017, pp. 877–896.

[63] M. A. Vega, V. Chandrasekar, J. Carswell, R. M. Beauchamp, M. R. Schwaller, and C. Nguyen, "Salient features of the dual-frequency, dual-polarized, Doppler radar for remote sensing of precipitation," *Radio Sci*., Vol. 49, 2014, pp. 1087–1105.

[64] M. R. Kumjian, "Principles and applications of dual-polarization weather radar. Part I: Description of the polarimetric radar variables," *J. Operational Meteor*., Vol. 1, No. 19, 2013, pp. 226–242.

[65] D. Giuli, "Polarization diversity in radars," *IEEE, Proceedings*, Vol. 74, 1986, pp. 245–269.

[66] D. S. Zrnic and A. V. Ryzhkov, "Observations of insects and birds with a polarimetric radar," *IEEE Transactions on Geoscience and Remote Sensing*, Vol. 36, No. 2, 1998, pp. 661–668.

[67] S. M. Bachmann and D. S. Zrnic, "Spectral density of polarimetric variables separating biological scatterers in the VAD display," *J. Atmos. Oceanic Technol*., Vol. 24, 2007, pp. 1186–1198.

[68] S. M. Bachmann and D. S. Zrnic, "Suppression of clutter residue in weather radar reveals birds' corridors over urban area," *IEEE Geosci. Rem. Sens. Lett.*, Vol. 5, No. 2, 2008, pp. 128–132.

[69] V. M. Melnikov, D. S. Zrnic, R. M. Rabin, and P. Zhang, "Radar polarimetric signatures of fire plumes in Oklahoma," *Geophys. Res. Lett.*, Vol. 35, 2008, p. L14815.

[70] V. M. Melnikov, D. S. Zrnic, R. M. Rabin, and P. Zhang, "Polarimetric radar properties of smoke plumes: A model," *J. Geophys. Res*., Vol. 114, 2009, p. D21204.

[71] T. A. Jones, S. A. Christopher, and W. Petersen, "Dual-polarization radar characteristics of an apartment fire," *J. Atmos. Oceanic Technol*., Vol. 26, 2009, pp. 2257–2269.

[72] D. J. Bodine, M. R. Kumjian, R. D. Palmer, P. L. Heinselman, and A. V. Ryzhkov, "Tornado damage estimation using polarimetric radar," *Wea. Forecasting*, Vol. 28, 2013, pp. 139–158.

[73] M. W. Long, "Radar Reflectivity of the Land and Sea," 3rd ed., *Artech House, Inc.*, 2001, 534 pp.

[74] D. S. Zrnić, V. M. Melnikov, and A. V. Ryzhkov, "Correlation coefficients between horizontally and vertically polarized returns from ground clutter," *J. Atmos. Oceanic Technol*., Vol. 23, 2006, pp. 381–394.

[75] D. S. Zrnic and A. V. Ryzhkov, "Polarimetric properties of chaff," *J. Atmos. Oceanic Technol*., Vol. 21, 2004, pp. 1017–1024.

[76] S. D. Howard, A. R. Calderbank, and W. Moran, "A Simple Signal Processing Architecture for Instantaneous Radar Polarimetry," *IEEE Transactions on Information Theory*, Vol. 53, No. 4, 2007, pp. 1282-1289.